Bolton, M. D. & Powrie, W. (1987). *Géotechnique* **37**, No. 3, 335–353

The collapse of diaphragm walls retaining clay

M. D. BOLTON* and W. POWRIE†

Five centrifugal model tests are reported which illustrate aspects of the collapse of stiff cantilever retaining walls embedded in overconsolidated clay. The drainage of a heavy fluid in flight was used to simulate the effects of excavation, following the establishment of a high initial groundwater level. Two modes of collapse were observed with unpropped walls. The temporary stability of walls with small penetration was interrupted by the hydraulic action of a water-filled crack opening on the retained side of the wall. The long-term rotational failure of walls of deeper penetration was also observed, involving distributed strains in 'active' and 'passive' zones which could lead ultimately to sliding on shear rupture surfaces. An analysis was developed based on admissible stress fields, with active and passive zones switching about a pivot point, so that the unpropped wall could satisfy the conditions of both moment and force equilibrium. A back analysis of the two sudden failures using an undrained strength based on the overconsolidation ratio was successful in matching the critical penetration ratio and pivot position observed in the tests. A drained analysis using ϕ' derived from triaxial and plane strain tests was equally successful in comparison with the data of long-term failure. A similar stress analysis for a wall propped at the top was shown to be conservative. This was thought to be due to the kinematic restraint of the prop which produced a rupture surface on the active side which was much steeper than those observed before. A back analysis of the observed failure mechanism generated a credible value of mobilized soil friction close to the peak observed in soil tests. This value also gave a consistent match for the bending moments and propping force measured in the test. Care must be taken to account for the possible effects of progressive failure. Critical state soil angles, with fully mobilized wall friction, can be anticipated to relate to the gross long-term deformation of walls. Loss of retained height and heave in the exacavation lead eventually to self-stabilization.

KEYWORDS: centrifuge modelling; clays; design; diaphragm walls; failure; stress analysis.

L'article décrit cinq essais de centrifugeuse effectués sur des modèles qui illustrent des aspects de la rupture de murs de soutènement cantilever rigides encastrés dans de l'argile surconsolidée. Le drainage d'un fluide lourd en vol fut employé pour simuler les effets de l'excavation, suivant l'etablissement d'un haut niveau initial d'eau souterraine. Deux modes de rupture furent observés avec des murs sans appui. La stabilité temporaire des murs avec peu de pénétration fut interrompue par l'action hydraulique d'une fente remplie d'eau qui s'ouvrait sur le côté amont du mur. On observa aussi la rotation à long terme des murs de pénétration plus profonde, conduisant à des déformations distribuées dans des zones 'actives' et 'passives' qui pourraient mener à la longue au glissement sur des surfaces de rupture de cisaillement. Une analyse fut développée basée sur des champs de contrainte admissibles, avec des zones actives et passives alternant autour de quelque point de pivotement, de sorte que le mur sans appui pouvait satisfaire aux conditions de l'équilibre des moments et des forces. Une analyse régressive des deux ruptures brutales, employant une résistance non-drainée basée sur le rapport de surconsolidation réussit à s'accorder au rapport critique de pénétration et à la position de pivotement observés au cours des essais. Une analyse drainée employant ϕ' dérivé d'essais triaxiaux et de déformation plane réussit également en comparaison avec les données de la rupture à long terme. Une analyse de contrainte analogue pour un mur appuyé en haut se montra un peu en deça de la realité, apparemment en raison de la restriction cinétique de l'appui, qui produisit sur le côté actif une surface de rupture beaucoup plus raide que celle observée auparavant. Une analyse régressive du mécanisme de rupture observé donna une valeur fiable du frottement du sol en mouvement ne différant pas beaucoup du pic observé lors des essais de sol. Cette valeur s'accorda bien aussi aux moments de flexion et à la force d'appui mesurés au cours de l'essai. Les champs de contrainte d'équilibre donnent une solution qui est en général sûre et fiable aux problèmes de l'instabilité des murs rigides encastrés. Les effets possibles de la rupture progressive doivent être pris en considération. On peut s'attendre à ce que les angles du sol dans l'état critique aient une relation avec la déformation totale à long terme des murs lorsque le frottement contre les murs est maximum.

Discussion on this Paper closes on 1 January 1988. For further details see p. ii.

* Cambridge University Engineering Department.
† King's College, London.

INTRODUCTION

Recent advances in construction technology, together with the high cost of city centre building land, have led to the increasing use of in situ retaining walls in connection with motorways and deep basements in urban areas. In many cases, the retained soil will be a clay, and existing codes of practice offer little guidance to the designer of a wall retaining such a soil. One of the principal uncertainties concerns the behaviour of the wall as the groundwater regime moves towards its long-term equilibrium state (Padfield & Mair, 1984).

The excess porewater suctions induced in the retained soil on excavation in front of the wall can take years or even decades to dissipate. In a $1:n$ scale model this time is reduced by a factor of n^{-2}; thus a model test represents the only method by which the long-term behaviour of a geotechnical construction in a soil of low permeability may be observed over a reasonably short period of time. Since the behaviour of the soil is heavily dependent on its stress state, it is desirable that the stresses at corresponding positions in the model and in the prototype should be the same. For a diaphragm wall, where self-weight stresses are of overriding significance, this can be achieved by subjecting the $1:n$ scale model to a radial acceleration of n times earth's gravity in a centrifuge. Gravitational forces in the prototype are replaced by centrifugal forces in the model.

A series of model tests has been conducted using the Cambridge geotechnical centrifuge as part of an investigation into the behaviour of diaphragm walls in clay. This Paper is concerned with the collapse of such walls. The behaviour of diaphragm walls before collapse will be the subject of a further publication.

DESIGN OF CENTRIFUGE MODEL

A typical centrifuge model is illustrated in Fig. 1 and represents a section of a long retaining wall. The length of the model wall section was 150 mm, corresponding to 18·75 m of a prototype wall at a scale of 1:125. For ease of back analysis, the deformation should take place under conditions of plane strain. The plane vertical boundaries perpendicular to the face of the model wall should therefore ideally have been rigid and frictionless. The centrifuge strong-box designed for the model tests had an aluminium alloy backplate 16 mm thick with two horizontal stiffening beams, and a Perspex front window 80 mm thick. To reduce friction to a minimum, the inside of the backplate was well lubricated with Molykote 33 silicone grease, and the inside of the Perspex window was sprayed with a mould release agent, Adsil, so that the view of the model was not obscured. It is estimated that the total restraining force due to friction from all sources would be less than 10% of the typical fully active force (including porewater pressure) acting on the retained side of the model wall above excavation level (Powrie, 1986).

The clay used in the model tests was speswhite kaolin, chosen principally because of its relatively high permeability $k = 0{\cdot}8 \times 10^{-9}$ m/s (Al Tabbaa, 1987). Kaolin powder was mixed under a partial vacuum with deionized water to a slurry with a moisture content of 120% (about twice the liquid limit). The slurry was then poured into a consolidation press, where it was gradually com-

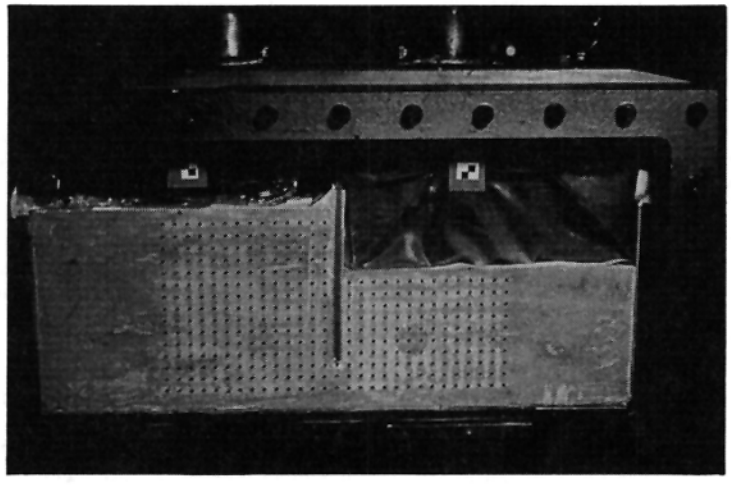

Fig. 1. Typical model (DWC 07) ready for testing in the geotechnical centrifuge

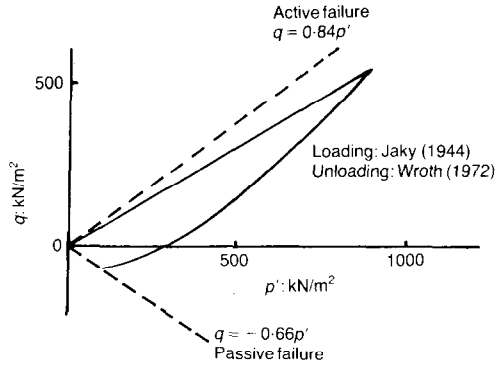

Fig. 2. Stress path in the consolidation press

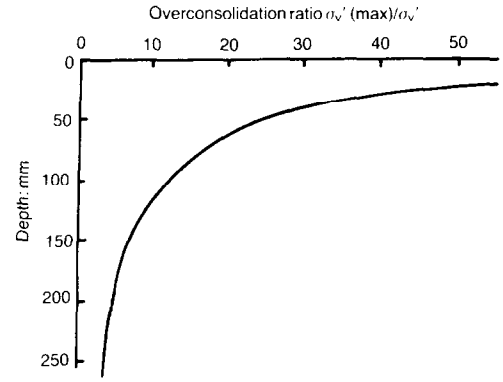

Fig. 3. Overconsolidation ratio versus depth in the model after reconsolidation in the centrifuge

pressed one dimensionally to a vertical effective stress of 1250 kN/m^2 and then unloaded to a vertical effective stress of 80 kN/m^2. The approximate stress path is shown in Fig. 2.

At an average effective stress of just under 100 kN/m^2, the clay was removed from the consolidation press and cut to receive the model retaining wall. The excavation was also made at this stage. The clay removed was replaced by a rubber bag containing zinc chloride solution, mixed to the same unit weight as the clay and filled to the level of the retained ground. The model was then transferred to the centrifuge strong-box and instrumented. After an initial reconsolidation period, during which the clay sample comes into equilibrium at 125g under its enhanced self-weight, the profile of overconsolidation ratio is as shown in Fig. 3. The vertical stress history corresponds to the removal by erosion of about 150 m of overlying soil and represents the conditions which would prevail in a typical overconsolidated clay deposit.

The peak angles of shearing resistance mobilized in triaxial compression tests on the speswhite kaolin were in the range 20·5–25·4° depending on the initial overconsolidation ratio of the sample and the type of test, as shown in Table 1. A value of $\phi'_{crit} = 22°$ or $M = 0{\cdot}84$ was selected as typical of the critical state strength in kaolin clays (Sketchley, 1973; Al Tabbaa, 1987). The peak drained angle of shearing resistance of the soil in the centrifuge model could be expected to be a few degrees higher than the corresponding drained triaxial strength. A reasonable upper estimate for the angle of shearing at mid-height in the model is 28°, corresponding to an overconsolidation ratio OCR of about 8.

The horizontal earth pressures require further consideration. Although the in situ lateral earth

Table 1. Triaxial compression tests on speswhite kaolin after one-dimensional precompression*

Test	1	2	3	4	5	6
Type of test	Drained	Drained	Undrained	Undrained	Undrained	Undrained
Moisture content as tested	—	—	40·5	40·5	40·6	44·9
Cell pressure: kN/m^2	450	461	454	353	412	400
Initial porewater pressure (back pressure): kN/m^2	340	351	340	218	196	275
p' at start of test: kN/m^2	110	110	114	135	212	125
p_0' (precompression): kN/m^2	890	890	890	890	890	287
p_0'/p'	8·1	8·1	7·8	6·6	4·2	2·3
ϕ'_{peak}: deg	25·6	23·7	23·0	24·6	22·1	20·5
Shear strain to failure: %	8·8	7·5	12·7	16·5	11·9	14·9
Type of failure	Rupture	Rupture	Rupture	Rupture	Squash	Squash
c_u: kN/m^2	—	—	76·3	84·7	121·9	47·3

* Rates of strain: undrained tests 1·23 mm/h, drained tests 1·76 mm/day.

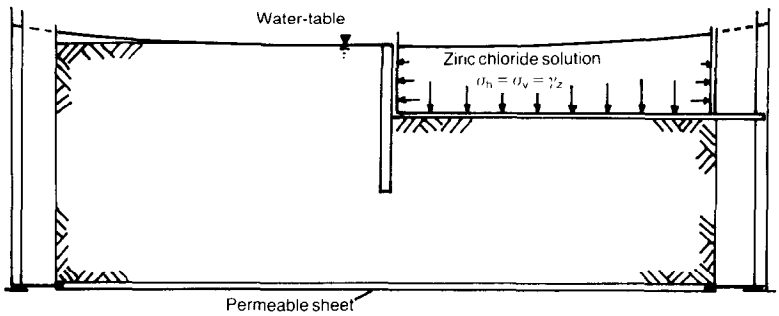

Fig. 4. Initial boundary conditions in the centrifuge

stresses in an overconsolidated clay deposit are likely to be high, the slurry trench phase of diaphragm wall construction is certain to alter them significantly. The exact effect of the casting of the wall will depend on the relative time-scales of wall construction and excess porewater pressure dissipation in the soil, the unit weight of the bentonite slurry, the unit weight of the concrete and the rapidity with which the concrete sets. An approximate analysis can be used to estimate limits to the likely pre-excavation lateral earth pressure coefficient (Powrie, 1985). In London clay, for example, the slurry trench phase might reduce an initial effective earth pressure coefficient of 2·0 to between 1·0 and 1·2. A pre-excavation lateral earth pressure coefficient of unity was therefore considered appropriate for the model diaphragm wall tests.

As the zinc chloride solution was mixed to the same unit weight as the soil it replaced, Fig. 4 illustrates that the boundary stresses were approximately consistent with this requirement after reconsolidation in the centrifuge. The establishment of $K_0 = 1$ in the heavy fluid need not imply that K_0 was exactly unity either behind the stiff wall or beneath the floor of the excavation. Bending moments measured in more flexible walls during the reconsolidation phase were rather small, however (Powrie, 1986), indicating that $K_0 = 1$ was quite closely achieved behind these walls, which were of similar stiffness to practical prototypes. The model therefore represents an artificial initial condition with porewater pressures in approximate equilibrium with a high groundwater table and with $K_0 \approx 1$. The provision of a valve-operated waste-pipe then enabled the zinc chloride solution to be drained from the rubber bag to simulate the excavation of the soil in front of the wall. As the fluid is drained, the lateral pressure reduction is proportional to the drop in level. A stress path with little initial horizontal stress reduction would apply beneath a real soil excavation: the transient process is thus modelled only approximately. Since the stress boundary conditions are correct both before and after excavation, and the time taken to drain the zinc chloride solution is comparatively short (2–5 min at model scale, corresponding to 3–8 weeks at prototype scale for a 10 m retained height), it is considered that the error introduced is negligible.

The layout of the model and the instrumentation is shown in Fig. 5. In all tests, the retained height of 80 mm in the model represented 10 m at prototype scale. The model walls were intended to be impermeable to groundwater and effectively rigid in bending. They were made of $\frac{3}{8}$ in aluminium alloy plate, giving an equivalent bending stiffness EI at prototype scale of approximately 10^7 kNm^2/m. The faces of the model walls were covered with a coating of resin 2 mm thick to protect the strain gauges and wires and to achieve a uniform and repeatable surface finish. The angle of friction between the resin and kaolin was tested by inserting a coated plate of aluminium in a shear box, with the surface of the resin flush with the plane of shearing. An effective angle $\delta = 21{\cdot}1°$ was recorded after about 1·5 mm of box displacement, dropping to 18·3° after a further 2·5 mm. It is consistent with the concept of critical states to infer that a surface on which there was an insignificant opportunity for dilation, but whose roughness was comparable with the particle size, might mobilize $\delta = \phi'_{crit}$. Such a surface might, as with other rupture surfaces, provide an opportunity for sliding leading to the development of residual friction conditions. Some further problems arising in the analysis of walls which suffer severe geometry changes are considered later. For the back analysis δ was not permitted to exceed ϕ'_{crit}, i.e. 22°.

In most tests, a full height groundwater level on the retained side of the wall was modelled and special silicone rubber wiper seals were used to prevent water from leaking between the edges of the wall and the sides of the strong-box. Stand-

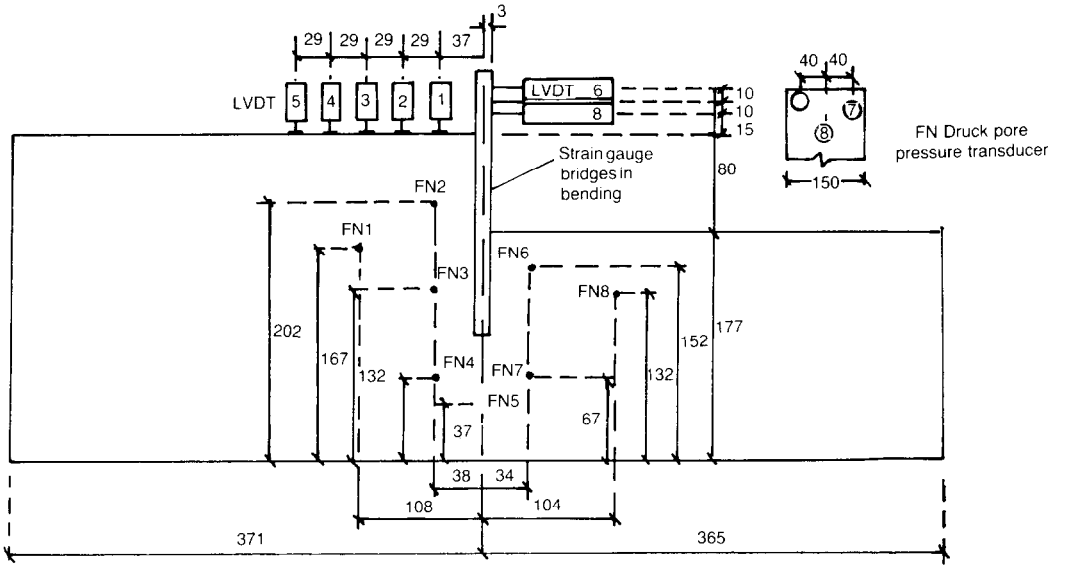

Fig. 5. Instrumentation of a typical model (dimensions in millimetres)

pipes with overflow outlets at fixed elevations were supplied with water from hydraulic slip rings to create constant head devices. By adjusting the supply flow rate, the elevation of water above the stand-pipe outlet could be finely adjusted. During the initial reconsolidation, water was supplied at the elevation of the ground surface to each of the ground surface, the base drainage sheet and the floor of the excavation. After 'excavation', solenoid valves were used to switch drainage lines to isolate the base drain and to keep the water level in the excavation drawn down to its floor. It can be shown that the presence of the isolated drainage sheet at the base of the model causes the steady seepage solution to mimic that of a much deeper soil stratum.

The general principles of centrifuge modelling are discussed in more detail by Schofield (1980), and the design of the model diaphragm wall tests is detailed in full by Powrie (1986).

THEORETICAL BACKGROUND

Diaphragm walls act as free or propped embedded cantilevers. For their stability they rely on a combination of the passive resistance of the soil in front of the wall and, usually, one or more rows of props or anchors. Assuming that a structural failure does not occur, an unpropped wall of penetration d will fail as a rigid body by rotation about an axis lying in the plane of the wall at an unknown distance z_p below the level of the excavation. Limiting stress distributions consistent with this mode of collapse are illustrated in Fig. 6 following the approach of Bolton (1979). It will be seen that the unknowns d and z_p will be determinable from the conditions of horizontal force and moment equilibrium. The introduction of the frictionless stress discontinuities against the wall and on the horizontal plane containing the pivot, as indicated in Fig. 6, guarantees that this method of analysis will underestimate the strength of the construction, assuming that the materials are plastic and that their strength has been correctly identified. The lateral earth pressures in each zone of soil at failure are given by the active and passive limits

$$\sigma_h' = \frac{1 - \sin \phi'}{1 + \sin \phi'} \sigma_v'$$

$$\sigma_h' = \frac{1 + \sin \phi'}{1 - \sin \phi'} \sigma_v'$$

respectively.

If the drop in excess head due to steady state seepage from the surface on the retained side into the excavation is taken as linear around the wall in the long term (Symons, 1983) the local hydraulic gradient will be

$$i = \frac{h}{h + 2d} \tag{1}$$

The vertical effective stress at depth z beneath the surface on the retained side can then be written

$$\sigma_v' = \gamma z - \gamma_w z + i\gamma_w z$$

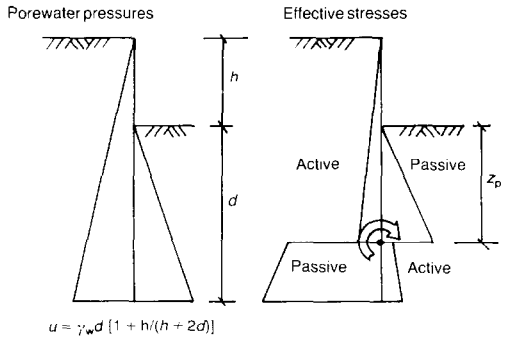

Fig. 6. Equilibrium stress analysis for the collapse of an unpropped wall

or

$$\sigma_v' = \gamma_r' z$$

where

$$\gamma_r' = \gamma - \gamma_w \frac{2d}{(h + 2d)} \tag{2}$$

Similarly, at depth z beneath the excavated surface

$$\sigma_v' = \gamma z - \gamma_w z - i\gamma_w z$$

or

$$\sigma_v' = \gamma_e' z$$

where

$$\gamma_e' = \gamma - \gamma_w \frac{2(h + d)}{(h + 2d)} \tag{3}$$

With an effective earth pressure coefficient K the total horizontal stress on the retained side becomes

$$\sigma_h = K\gamma_r' z + \gamma_w z - i\gamma_w z$$

or

$$\sigma_h = \gamma z - (1 - K)\gamma_r' z \tag{4}$$

On the excavated side, similarly

$$\sigma_h = \gamma z - (1 - K)\gamma_e' z \tag{5}$$

Respecting the switch in active and passive conditions about the pivot, the equilibrium of horizontal forces on the wall in Fig. 6 can be written

$$\frac{1}{2}\gamma(h + d)^2 - \frac{(1 - K_p)}{2}\gamma_r'(h + d)^2 - \frac{(K_p - K_a)}{2}\gamma_r'(h + z_p)^2 = \frac{1}{2}\gamma d^2 - \frac{(1 - K_a)}{2}\gamma_e' d^2 + \frac{K_p - K_a}{2}\gamma_e' z_p^2$$

or

$$(h + d)^2[\gamma + (K_p - 1)\gamma_r'] - (h + z_p)^2\gamma_r'(K_p - K_a) - d^2[\gamma + (K_a - 1)\gamma_e'] - z_p^2\gamma_e'(K_p - K_a) = 0 \tag{6}$$

Moment equilibrium about the wall crest gives

$$\frac{1}{3}\gamma(h + d)^3 - \frac{(1 - K_p)\gamma_r'}{3}(h + d)^3 - \frac{(K_p - K_a)\gamma_r'}{3}(h + z_p)^3 = \frac{1}{2}\gamma d^2\left(h + \frac{2d}{3}\right) - \frac{(1 - K_a)\gamma_e' d^2}{2}\left(h + \frac{2d}{3}\right) + \frac{(K_p - K_a)\gamma_e' z_p^2}{2}\left(h + \frac{2z_p}{3}\right)$$

or

$$(h + d)^3[\gamma + (K_p - 1)\gamma_r'] - (h + z_p)^3\gamma_r'(K_p - K_a) - d^2\frac{(3h + 2d)}{2}[\gamma + (K_a - 1)\gamma_e'] - z_p^2\frac{(3h + 2z_p)}{2}\gamma_e'(K_p - K_a) = 0 \tag{7}$$

Equations (6) and (7) can readily be satisfied iteratively. It is necessary first to find the depth z_m below the excavation, at which the shear force in the wall first passes through zero.

$$\frac{1}{2}\gamma(h + z_m)^2 - \frac{(1 - K_a)}{2}\gamma_r'(h + z_m)^2 = \frac{1}{2}\gamma z_m^2 - \frac{(1 - K_p)}{2}\gamma_e' z_m^2$$

from which

$$\frac{z_m}{h} = \left\{\left[\frac{1 + (K_p - 1)\gamma_e'/\gamma}{1 - (1 - K_a)\gamma_r'/\gamma}\right]^{1/2} - 1\right\}^{-1} \tag{8}$$

An appropriate procedure for the solution of equations (6) and (7) is then to select an initial increment Δd for d, say $z_m/8$, and then to permit d to increase from $z_m + \Delta d$, increment by increment. At each stage a value of z_p that is consistent with force equilibrium can be found using the quadratic equation (6). The error in moment balance can then be calculated from equation (7). Incrementing must continue until the error changes sign. From there onwards the increment must be halved each time, and its sign should be reversed whenever the sign of the error reverses. When the increment Δd is a sufficiently small proportion of z_m, say $z_m/1024$, the calculation can stop and both d and z_p can be reported.

Elementary routines such as this are now widely appreciated and can be implemented

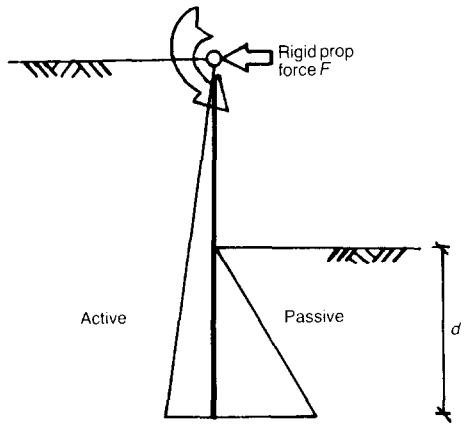

Fig. 7. Equilibrium stress analysis for the collapse of a wall propped rigidly at the crest

immediately on any microcomputer. Given this simplicity it is perhaps surprising that approximate methods such as the 'fixed earth support' assumption, in which the wall is taken to be 'pinned' at its foot by soil forces, are still considered necessary.

The corresponding limit state calculation for a wall propped rigidly at the crest is illustrated in Fig. 7. Assuming that the props do not fail, the position of the axis of rotation is defined. The two unknowns are then the depth of penetration required for moment equilibrium about the prop and the force exerted by the prop to keep the system in horizontal equilibrium. Solution of the equilibrium equations is simpler in this case.

If the wall is rough, an additional complexity is introduced into the stress field calculation. The presence of shear stresses at the soil–wall interface necessitates a rotation of the principal stress directions in the soil adjacent to the wall. For a wall where there is only one zone of soil at failure (either active or passive), the integration of the equilibrium equation from an assumed boundary condition can lead to a modified earth pressure coefficient $\sigma_h'/\gamma' z$ (Caquot & Kerisel, 1948). The term $\gamma' z$ does not then represent the vertical stress at a point, since wall friction will have affected it, but is purely a normalizing term taken as $\gamma z - u$ where u is itself taken to be proportional to z. The application of these earth pressure coefficients to the limit state calculation for an unpropped wall (Fig. 6) gives an indication of the likely effect of friction at the soil–wall interface, but this procedure has no rigorous justification since the stress distribution on the horizontal plane through the pivot is not properly dealt with.

It is also assumed that the bearing stresses on the base of the wall are able to support the self-weight of the wall, and any reasonable friction on the faces of the wall, without contributing significantly to the equilibrium of horizontal forces or moments. It can be shown that this idealization, corresponding to the neglect of wall thickness, leads to a slightly conservative analysis.

UNPROPPED WALLS OF SHALLOW PENETRATION

Throughout this Paper, test data are presented at prototype scale according to the appropriate scaling rules. For example, elapsed time has been multiplied by a factor of 125^2 and measurements of length by 125. No account has been taken of differences in soil properties between a model and a prototype. The results presented in this way relate to a prototype wall retaining 10 m of speswhite kaolin. To relate test duration to the time-scale of consolidation, a characteristic drainage path length was chosen equal to the average depth of the soil on either side of the wall, $d = (32{\cdot}1 + 22{\cdot}1)/2 = 27{\cdot}1$ m at prototype scale. The settlements measured during reconsolidation in the centrifuge indicated a consolidation coefficient c_v ($= E_0' k/\gamma_w$) of about 2·5 mm^2/s. Dimensionless time factors $T_v = c_v t/d^2$ are quoted on this basis although the geometry of transient flow was quite complex.

Taking $\phi'_{crit} = 22°$, the limit equilibrium stability analysis illustrated in Fig. 6 indicates that large depths of penetration are required to retain 10 m of saturated kaolin with an unpropped wall in the long term. Depending on the degree of soil–wall friction invoked, the depth of penetration required to achieve a factor of safety of unity is between 29 m and 42·5 m for a full height groundwater level behind the wall and steady state seepage into the excavation. Under these groundwater conditions, unpropped walls of 5 m (test DWC 06) and 10 m (test DWC 09) penetration failed almost immediately on excavation. The initial soil deformations were so large that a tension crack opened between the wall and the retained soil. Surface water was led towards the settlement trough behind the wall, filling the crack and pushing the wall over almost instantaneously. The retained ground was left standing in a cliff as shown in Fig. 8.

The short-term equilibrium of these walls of shallow penetration is dependent on the generation of large porewater suctions near the wall and may additionally require the transmission of tensile stress at the soil–wall interface. If the penetration is too small, the wall rotation will be relatively large and the soil–wall interface will be incapable of transmitting the necessary tension: crack propagation will lead to sudden failure. The mechanism of collapse involves plastic deforma-

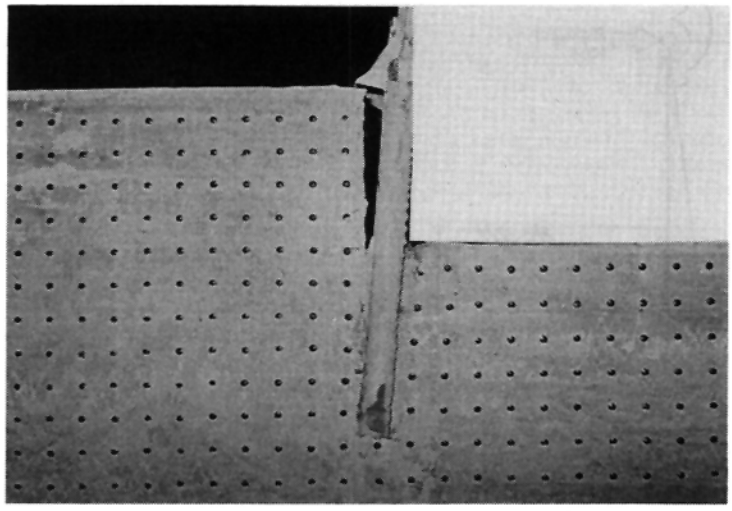

Fig. 8. Flooded tension crack failure of test DWC 09

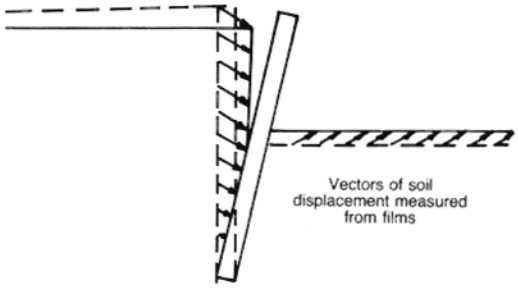

Fig. 9. Collapse mechanism for a water-filled crack behind unpropped walls

tion of the soil below the zone within which the porewater suctions are sufficiently high to maintain the stability of a vertical cut. This is illustrated in Fig. 9.

Although they relate to the instant just before outright collapse, the data on soil deformations measured from films (Fig. 10) support this view. The arrowheads representing the ends of the displacement vectors nearest the wall in the retained soil require two distinct straight lines to join them. This indicates that the wall must have broken away from the soil on the retained side above the level of the change in slope.

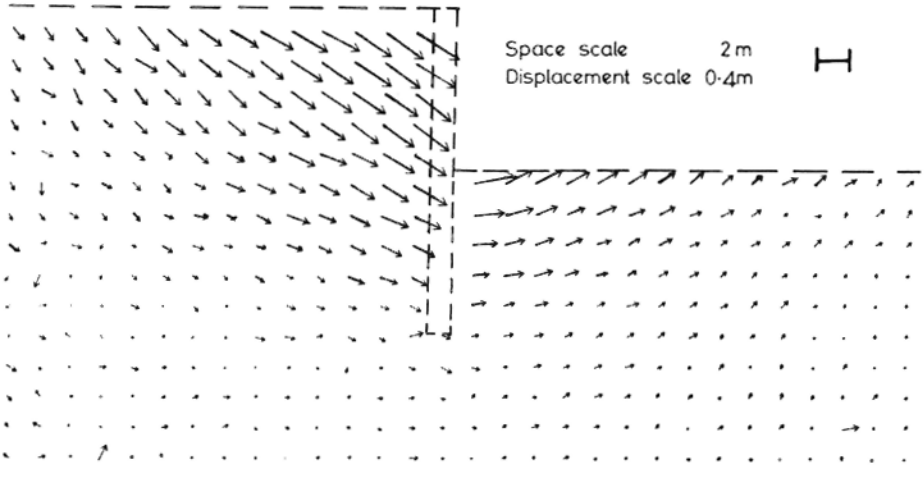

Fig. 10. Soil movements during excavation, test DWC 09

Although the undrained behaviour of these walls can be described in terms of effective stresses and local excess porewater suctions, the use of an analysis based on total stresses is more convenient. It is often sought (e.g. Wroth (1984)) to estimate the end point of an undrained test from its starting point. The undrained shear strength of the soil can be related to its stress history by a relationship of the form

$$\frac{c_u/\sigma_{v_1}'}{(c_u/\sigma_{v_1}')_{nc}} = (OCR)^m \qquad (9)$$

where c_u is the undrained shear strength, σ_{v_1}' is the vertical effective stress at the start of the test and the overconsolidation ratio OCR is based on vertical effective stresses. The subscript nc denotes the normally consolidated state (OCR = 1), and the value of the constant m can either be derived theoretically (Wroth, 1984) or determined experimentally from laboratory test data.

The value of c_u would be expected to depend on the effective stress path followed by the soil during the undrained test. Thus a prediction of c_u based on a series of triaxial compression tests is strictly inapplicable to a plane strain event where the effective stress path is rather different. None the less, the triaxial test data presented in Fig. 11 enable an approximate profile of undrained shear strength to be determined (with $m = 0{\cdot}49$) according to equation (9), for the clay after reconsolidation in the centrifuge.

The undrained shear strength profile based on the nominal (full height) pre-excavation groundwater conditions for the clay used in the centrifuge tests is shown in Fig. 12. Generally, a slightly depressed groundwater level was indicated by the measurements of porewater pressure near the wall. The undrained shear strength profile based on the pre-excavation porewater pressures measured in a typical centrifuge test (DWC 08) is also

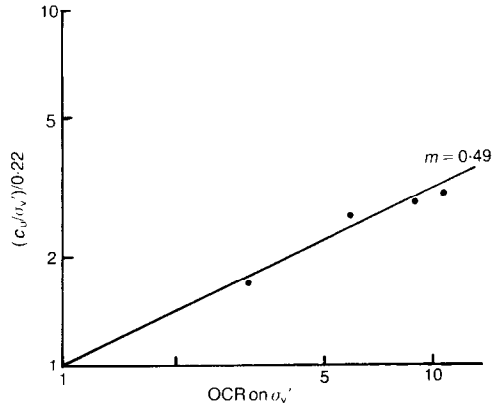

Fig. 11. Undrained triaxial shear strength versus log (OCR)

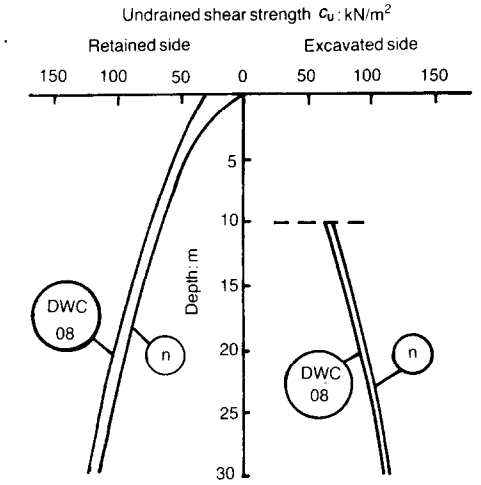

Fig. 12. Profiles of undrained strength versus depth

shown in Fig. 12. For the current analysis, the difference between them is not significant, and the nominal shear strength profile (labelled n in Fig. 12) has been used for ease of computation.

The short-term stability of the wall can be assessed using a lower-bound approach based on permissible stress fields after the fashion of Fig. 6, but incorporating a uniform undrained strength c_u as shown in Fig. 13. It is necessary to take into account the possible depth h_c of a vertical tension crack on the retained side. The vertical stress σ_v in the soil near the base of such a crack is γh_c, so that if the crack is dry and the horizontal stress $\sigma_h = 0$ the criterion of limiting shear stress will give

$$\sigma_h = \sigma_v - 2c_u = \gamma h_c - 2c_u = 0$$

The critical dry crack depth is therefore $h_c = 2c_u/\gamma$ as shown in Fig. 13. If the crack were able to fill with water to the surface of the clay the horizontal stress would be hydrostatic, so that

$$\sigma_h = \sigma_v - 2c_u = \gamma h_c - 2c_u = \gamma_w h_c$$

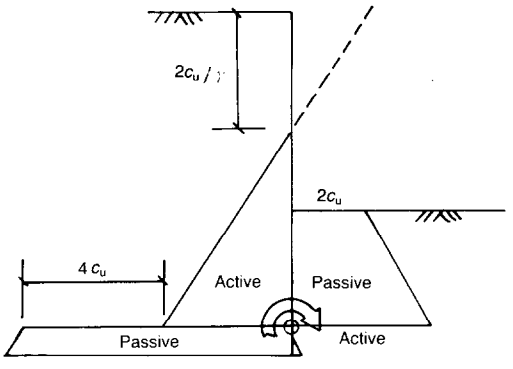

Fig. 13. Equilibrium stress analysis for the collapse of a wall in undrained clay with a dry tension crack

leading to a critical wet crack depth of $h_c = 2c_u/(\gamma - \gamma_w)$. Taking the increase in c_u with depth from profile n in Fig. 12 and using $\gamma = 17.5$ kN/m^3 the theoretical crack depths would be 5.7 m dry and 31 m flooded.

In the absence of water to fill cracks, therefore, a 10 m wall in overconsolidated clay would require a small penetration of about 2 m to maintain short-term equilibrium. If a crack between the soil and the wall could flood, however, it could remain open to considerable depth transferring hydraulic thrust to the wall. The wall could be forced outwards as the crack widened provided that the rate of inflow was sufficient to maintain the head in the crack. An analysis has been conducted of the limiting equilibrium of walls in clay of uniform strength, with a water-filled crack in the active zone above the pivot point, as indicated in Fig. 14. The wall height and pivot position were adjusted until global equilibrium of forces and moments was achieved. The results are shown in Fig. 15 in which the limiting penetration ratio d/h is plotted against stability number $\gamma h/c_u$ for various soil unit weights. In each case the height of the pivot position above the base was about one-twelfth of the total wall height, i.e. $0{\cdot}08(h + d)$, and the height above the base of the position of zero shear force and maximum bending moment was approximately $0{\cdot}25(h + d)$.

Taking $\gamma = 17{\cdot}5$ kN/m^3 and $c_u = 83$ kN/m^2 for a wall of height $h = 10$ m, Fig. 15 indicates a limiting penetration $d = 13{\cdot}5$ m at $\gamma h/c_u = 2{\cdot}1$. This offers a flooded crack depth of $0{\cdot}92 \times 23{\cdot}5 = 21{\cdot}6$ m down to the pivot, which happens to correspond to the theoretical maximum value. Reference back to Fig. 12 also shows that $c_u = 83$ kN/m^2 is expected in the centrifuge model tests at 5 m depth beneath the excavation, which coincides with the centre of the penetration zone. An independent calculation taking into account the variation in c_u with depth confirmed the prediction that about 14 m was the limiting penetration at which a water-filled crack could no longer cause complete failure of the wall.

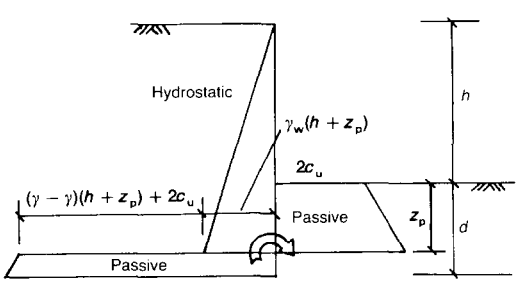

Fig. 14. Equilibrium stress analysis for the collapse of a wall in undrained clay with a water-filled tension crack to depth $h + z_p < 2c_u/(\gamma - \gamma_w)$

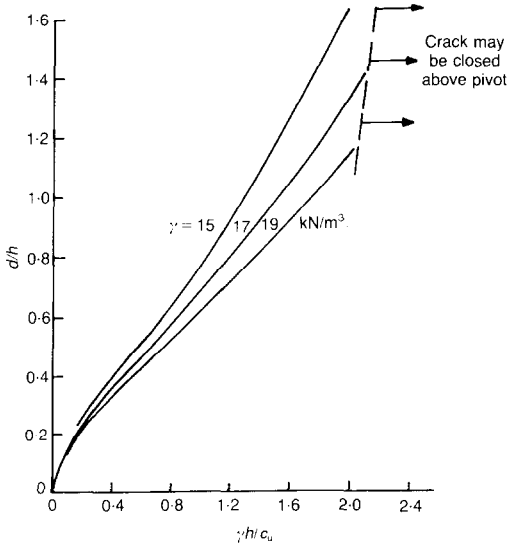

Fig. 15. Limiting penetration ratios for walls with water-filled cracks

The short-term behaviour of these two unpropped model walls is thus explained, at least qualitatively. As would be expected from this analysis, the wall of 5 m penetration (DWC 06) failed almost immediately after excavation owing to the effect of a flooded tension crack. The short delay, 9 weeks at prototype scale (corresponding to $T_v = 0{\cdot}02$), between the completion of the excavation and the failure of the wall of test DWC 09 with a 10 m penetration must be taken to confirm that the analysis of Fig. 15 is conservative, and that some initial deformation was required before the tension crack could open. The tension crack shown in Fig. 8 extends below the depth of the excavation, as required in Fig. 14. However, the active soil in Fig. 10 clearly tended to follow the wall as it rotated away, thereby reducing the available depth of a crack compared with the theory for rigid–perfectly plastic materials. Considering the apparent success of the simpler theory in correctly discriminating a change in failure mode between penetrations of 10 m and 15 m, it is not considered fruitful to attempt a more refined elasto-plastic stability analysis.

UNPROPPED WALLS OF DEEPER PENETRATION

With a nominally full height groundwater level on the retained side, the behaviour of two further unpropped walls of 15 m (DWC 07) and 20 m (DWC 08) penetration was investigated.

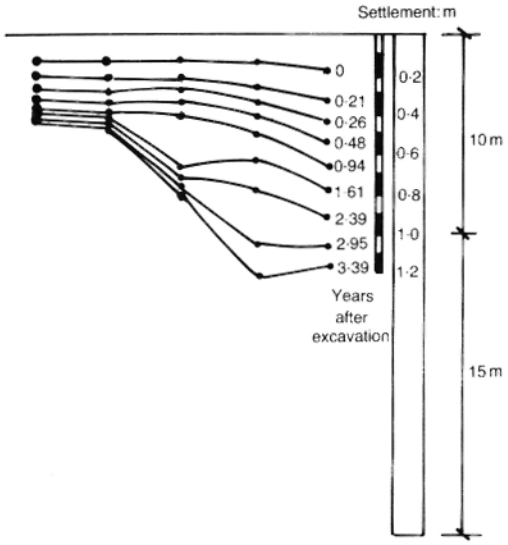

Fig. 16. Soil settlement profiles, test DWC 07

The wall of 15 m penetration (test DWC 07) suffered large movements on excavation but apparently remained in contact with the soil. Wall movement and soil deformations continued after excavation with no sign of abatement. Soil surface profiles at various stages after excavation are shown in Fig. 16: the deformations were clearly influenced by the development, some time after excavation, of one or more slip surfaces. Fig. 17 illustrates the final pattern of rupture lines. The presence of numerous small ruptures at angles of approximately $90° - \phi'$ to the main slip surfaces is interesting.

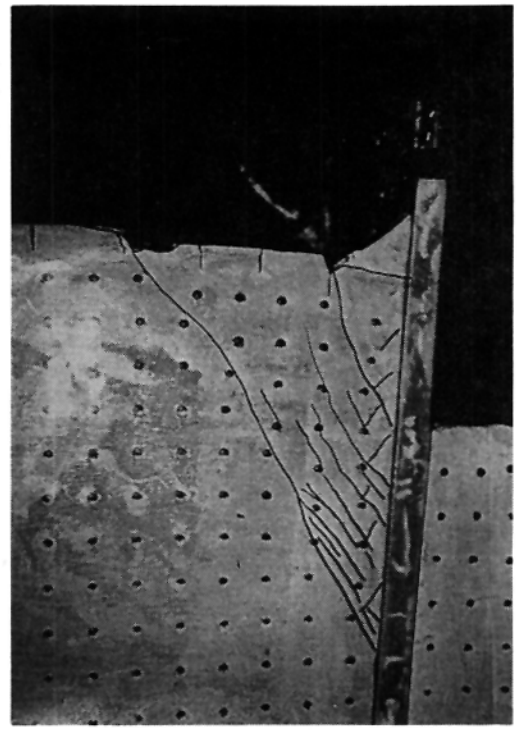

Fig. 17. Post-flight view, test DWC 07

The soil movements measured from photographs taken during excavation are shown in Fig. 18. The arrowheads representing the ends of the column of displacement vectors nearest to the wall in the retained soil can all be joined by a

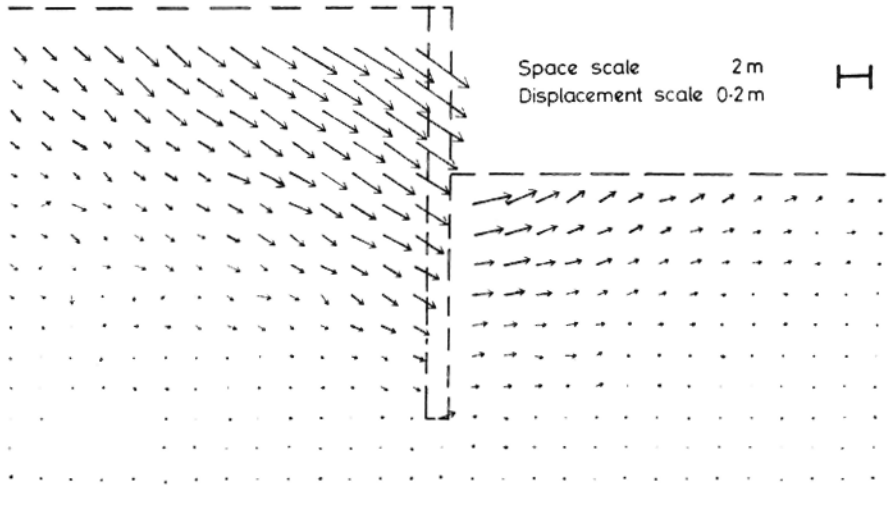

Fig. 18. Soil movements during excavation, test DWC 07

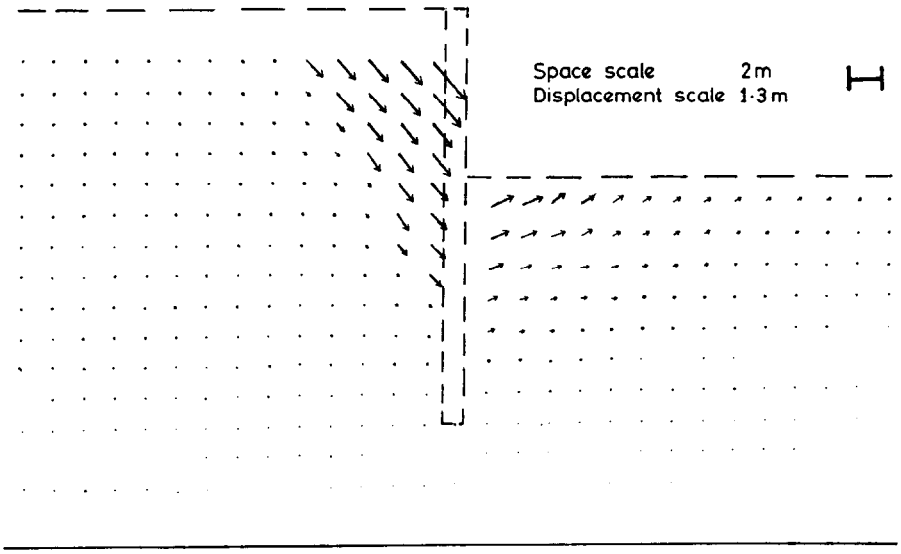

Fig. 19. Post-excavation soil movements, test DWC 07

single straight line, and similarly for the column of displacement vectors nearest to the wall on the excavated side, and the two lines are parallel. Unlike the tests on shallower walls (tests DWC 06 and DWC 09), the soil displacements are compatible with the movement of the rigid wall. The soil and the wall remained in contact, and a tension crack did not develop. The boundaries of significant soil movement are quite clearly defined on both sides of the wall, there being little movement outside 45° triangles drawn from the base of the wall.

In the long term, the most significant soil displacements on the retained side of the wall resulted from the sliding of a triangular block of soil along the main slip surface. This is confirmed by Fig. 19, which illustrates the soil movements measured from films which occurred over a period of nearly 7 years (at prototype scale) after excavation had been completed, corresponding to $T_v = 0{\cdot}75$.

The deepest wall had a penetration of 20 m (test DWC 08) which, with a full height groundwater level behind it, was still insufficient to prevent unacceptably large soil deformations. Soil surface profiles are illustrated in Fig. 20. At the conclusion of the test (corresponding to $T_v = 1{\cdot}5$ after about 14 years at prototype scale) movement was still apparent albeit at a much lower rate than in test DWC 07 (15 m penetration). Perhaps the major difference between the behaviour of the 20 m wall and that of the 15 m wall was that the 20 m wall was sufficiently deep to prevent or postpone the development of slip surfaces. This was confirmed by radiographs taken after the test. The rigid base only 2·25 m below the foot of the prototype of DWC 08 with 20 m penetration might have influenced the results. However, Figs 10, 18 and 19 indicate that displacements below the foot of the shallower walls are apparently negligible, so the effect cannot be significant.

As indicated by the short-term total stress analysis used for the shallower walls of tests DWC 06 and DWC 09, the unpropped walls of 15 m (DWC 07) and 20 m (DWC 08) embedment were sufficiently deep to prevent a sudden col-

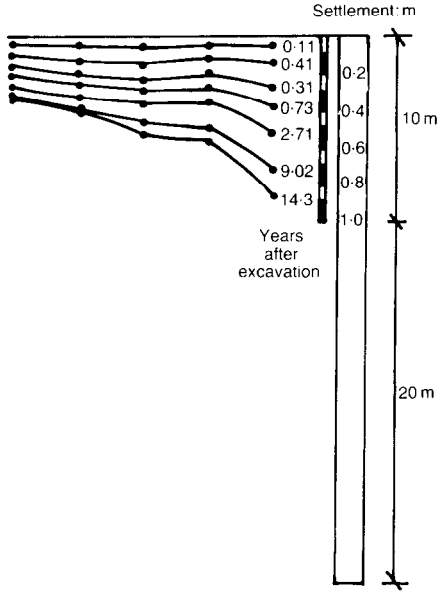

Fig. 20. Soil settlement profiles, test DWC 08

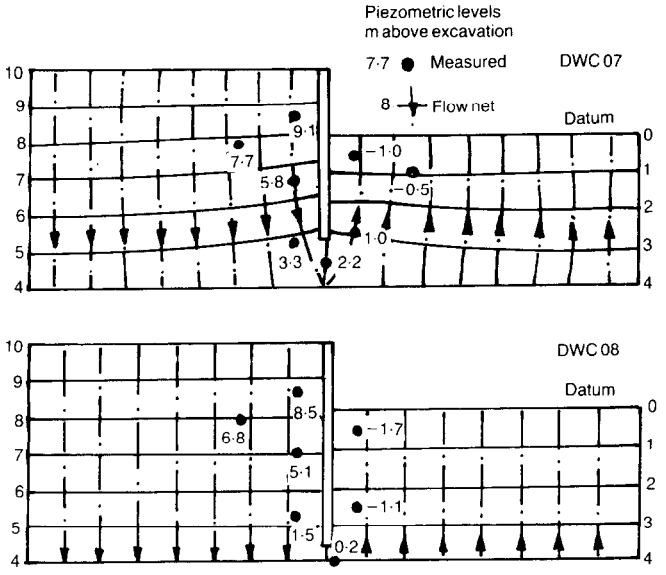

Fig. 21. Piezometric levels compared with ideal steady flow nets

lapse. The long-term behaviour of these walls is best discussed in terms of effective soil stresses and porewater pressures.

The piezometric levels measured near the end of each test are compared with theoretical isotropic steady flow nets in Fig. 21 and the corresponding porewater pressures adjacent to the wall are shown in Fig. 22. The idealized porewater pressure distributions fitted to the data and used for analysis are also shown. In Figs 21 and 22, the wall geometry is shown in its original (undeformed) state. In tests DWC 07 and DWC 08, the long-term soil movements were sufficiently large to warrant back analysis based on the deformed geometry. Since the porewater pressure transducers are unlikely to move with respect to the surrounding soil, the porewater pressures at the soil surfaces and at the bottom of the wall were taken to be those indicated in Fig. 22.

The ultimate equilibrium of each wall at an instant near the end of the test was investigated using the assumed distribution of the effective soil stresses illustrated in Fig. 23. The method of analysis was analogous to the procedure outlined earlier for the derivation of a just safe penetration d for a wall mobilizing its full angle of shearing ϕ'. On this occasion, the penetration d was known and the conditions of horizontal and moment equilibrium analogous to equations (6) and (7) could be used with the smoothed water pressure observations to make deductions about the mobilized angle of shearing. As before, the depth z_p of the required pivot could also be derived.

An extra degree of freedom is attached to the situation of Fig. 23 compared with that of Fig. 6. There is the possibility that the mobilized angles ϕ'_{mob} need not now be at any limit. Nevertheless, the large deformations apparent in tests DWC 07 and DWC 08 encouraged the further assumption

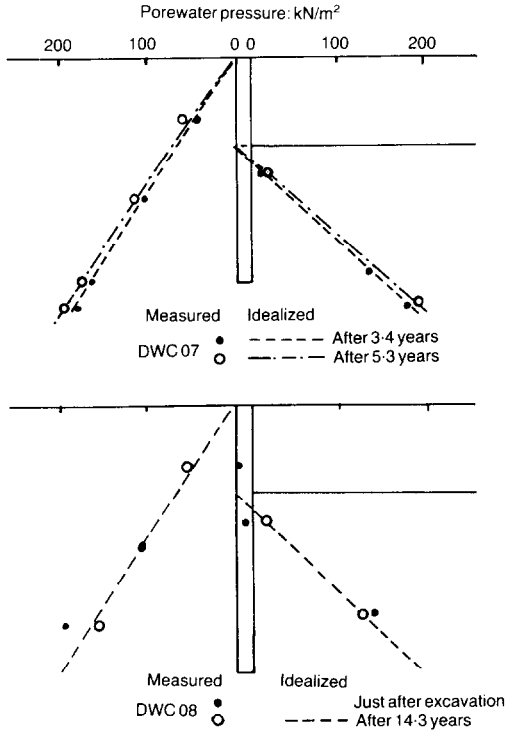

Fig. 22. Porewater pressures near the wall

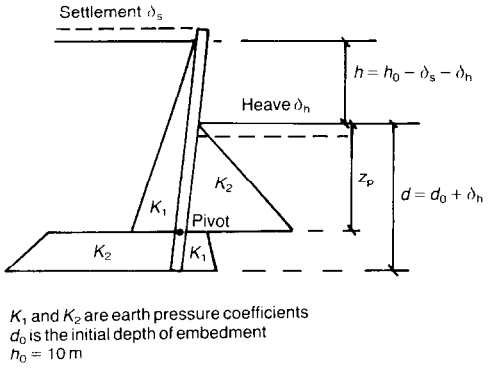

Fig. 23. Stress distribution assumed in the equilibrium analysis of unpropped walls

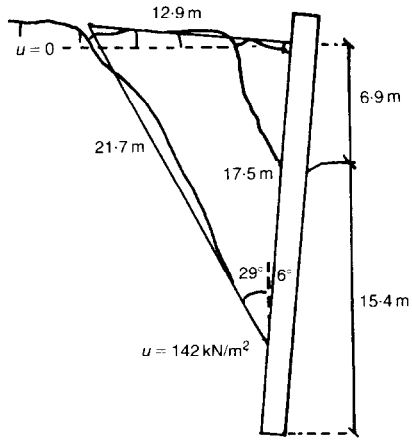

Fig. 24. Idealized sliding wedge, test DWC 07

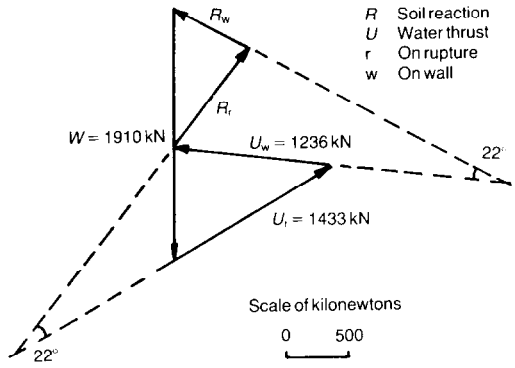

Fig. 25. Polygon of forces for a sliding wedge, test DWC 07 (all forces are per metre run)

that ϕ' is mobilized identically everywhere. Similarly, the large relative movements of soil against the wall indicated that it might be reasonable to take wall friction as fully mobilized with $\delta = \phi'$. The procedure was to assume as an initial value that $K_1 = K_a = 0{\cdot}387$ from Caquot & Kerisel (1948) with $\delta_1 = \phi_1' = 22°$, the critical state value. K_2 and z_p could then be calculated. The same tables could then be used to determine the value $\phi_2' = \delta_2$ corresponding to K_2 in the passive condition. Iteration was then employed to alter K_1 and the corresponding K_2 until $\phi_1'\ (=\delta_1) \approx \phi_2'\ (=\delta_2)$. These results are listed in Table 2, together with the corresponding value of z_p.

In test DWC 07 the back analysis indicated a mobilized angle of shearing almost identical with the critical state angle at 21·7°. Furthermore, the analysis generated a pivot point 14 m below the excavation, whereas a best straight line fitted to the cumulative displacements indicated a pivot at about 13·5 m depth and the main rupture surface intersected the wall at about 10 m depth. In test DWC 08 the angle ϕ' required for equilibrium was about 19·7°, slightly smaller than the critical state angle. This is consistent with the less damaging deformation and lack of any clear rupture surface. The wall was, nevertheless, clearly on the verge of limiting equilibrium. The method of stress analysis was apparently successful in the back analysis of states of collapse.

In test DWC 07 (15 m penetration), a definite rupture developed on the active side, so an alternative equilibrium analysis of the sliding wedge can be used to determine the effective soil thrust. The idealized wedge used in this analysis is shown in Fig. 24 and the force polygon in Fig. 25. It has been assumed that the critical state angle of friction of 22° was mobilized both on the rupture surface and at the wall. This is reasonable because of the magnitude of the soil strain which had occurred close to these planes. The effective

Table 2. Back analysis of the long-term equilibrium of unpropped walls

Time factor T_v after completion of excavation	Altered geometry		Active zones		Passive zones		z_p: m
	h: m	d: m	K_1	$\phi'\ (=\delta)$: deg	K_2	$\phi'\ (=\delta)$: deg	
DWC 07 0·61	6·9	15·4	0·39	21·7	3·18	21·7	13·9
DWC 08 1·5	8·7	20·4	0·41	19·7	2·76	19·7	18·4

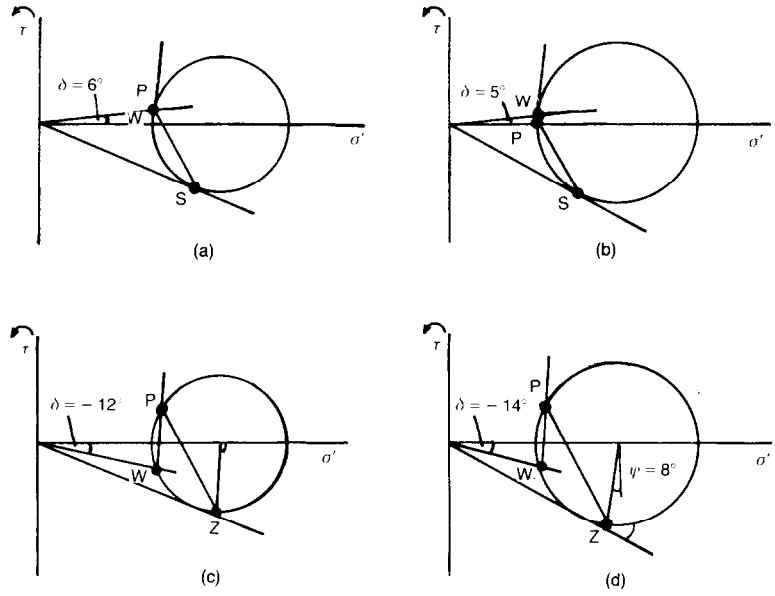

Fig. 26. Hypothetical Mohr circles of effective stress at rupture, test DWC 07

soil stresses and porewater pressures were taken to vary linearly with depth.

This analysis gives an effective horizontal thrust of 580 kN/m (excluding the porewater pressures) due to the soil contained within the sliding wedge, compared with 542 kN/m if the lateral earth pressure coefficient of 0·387 is taken from Table 2. Bearing in mind the approximations made in each analysis, this discrepancy is not sufficiently large to indicate any significant inconsistency.

Finally, it is interesting to speculate on the stress conditions in test DWC 07 at the instant the main rupture surface developed at $T_v = 0{\cdot}41$ or about 2 years of prototype time before the final configuration analysed in Table 2. At this stage, the height of soil supported had already reduced from 10 m to 8·0 m, the penetration could be taken to be 15·4 m and the wall was inclined at 6° to the vertical, corresponding to a shear strain in the active zone of roughly 20%.

Rupture surfaces may develop along a plane of maximum stress obliquity, a zero-extension line, or some intermediate direction. Fig. 26 shows four Mohr circles of effective stress constructed under various assumptions

(*a*) $\phi' = \phi'_{crit} = 22°$ (rupture on plane of maximum stress obliquity *S*)

(*b*) $\phi' = \phi'_{max} = 28°$ (rupture on plane of maximum stress obliquity *S*)

(*c*) $\phi' = \phi'_{crit} = 22°$ (rupture on plane of zero extension *Z* ($\psi = 0$), taking principal stress and plastic strain increment directions to be coincident)

(*d*) $\phi' = \phi'_{max} = 28°$ (rupture on plane of zero extension *Z* ($\psi = 8°$), taking principal stress and plastic strain increment directions to be coincident).

The angle of dilation ψ for (*c*) and (*d*) was selected in approximate conformity with Rowe's stress dilatancy theory using $\psi = (\phi' - \phi'_{crit})/0{\cdot}8$ (Bolton, 1986). It will be seen that the pole P for planes has been located in each case using 29° as the inclination to the vertical axis of the observed rupture as it approached the wall. The corresponding stress state W on the wall was derived using the 6° angle of tilt.

In Figs 26(c) and 26(d) the shear angle on the wall becomes negative, implying an upward movement of soil relative to the wall, which can be discounted. Apparently, the range of situations corresponding to (*a*) through (*b*) is both kinematically and statically admissible. The wall apparently generated only a small angle of friction $\delta \approx 5°$ on the active side at the instant of rupture.

A global analysis after the fashion of Fig. 23, and using porewater pressures corresponding to the estimated time of first rupture, could be satisfied by the universal values $\phi = 28°$ and $\delta = 9°$. This situation corresponds to the mobilization of a peak strength about 3° larger than that observed either in drained triaxial tests or undrained plane strain tests: this is quite reasonable. The analysis implies that the peak soil strength is initially mobilized at strains that are insufficient to create any substantial wall friction. Apparently, the wall friction increased as the soil

softened towards its critical state strength, sliding on the ruptures which had formed.

Despite the assumptions and approximations made in the analyses presented in this section, the data are encouragingly consistent. The long-term behaviour and collapse of the unpropped walls can be described and explained using simple conventional models of soil behaviour.

RIGID WALL PROPPED AT CREST

The behaviour of a wall of 5 m penetration propped at the crest was investigated in test DWC 11. The analysis illustrated in Fig. 7 indicates that, with a full height groundwater level on the retained side, such a wall would require a depth of embedment of between 13·5 m ($\delta = \phi'$) and 20 m ($\delta = 0$) to achieve a factor of safety of unity. The development of rupture surfaces in the soil at $T_v = 0{\cdot}21$ approximately 2 years after excavation was not surprising therefore.

The rupture pattern is illustrated in Fig. 27. The main rupture surface is reminiscent of the logarithmic spirals observed by Lord (1969) in an investigation of the failure of propped model walls retaining sand. In addition, there are numerous indications of secondary rupture of the type observed in test DWC 07. At first sight, the main rupture suface near the top of the wall on the retained side is unusually steep, but this is due to the kinematic restraint imposed by the prop. In the absence of dilation, pure sliding would be impossible along a plane surface in any other direction.

Soil settlement profiles are illustrated in Fig. 28. The influence of the ruptures is manifest in the differential settlements which started within 2 years after excavation. The later settlement profiles indicate that slip had occurred along the main rupture surfaces.

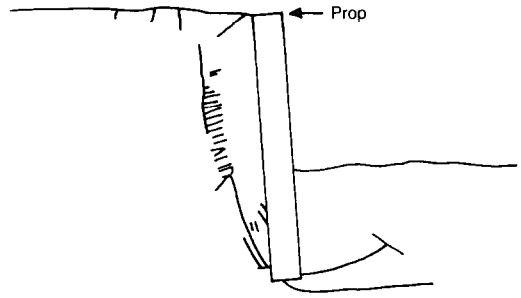

Fig. 27. Rupture pattern, test DWC 11

The analysis of the short-term stability of unpropped walls presented earlier can easily be extended to include walls propped at the crest. The penetration must be sufficiently deep to ensure that the moment about the prop of the available passive resistance is greater than that of the active disturbing pressure: horizontal equilibrium is now guaranteed by the prop. A depth of penetration of 0·5 m is sufficient—unless free water can find its way to the soil–wall interface and exert a hydrostatic pressure, in which case a penetration of up to 4·4 m could be required. This, apparently, did not happen.

The long-term behaviour observed in test DWC 11 will be analysed by considering the static equilibrium of the zones of soil bounded by the rupture surfaces. For this, the idealized rupture surfaces and porewater pressures shown in Figs 29 and 30 corresponding to $T_v = 0{\cdot}79$ after 7·4 years will be used. In reality, the long

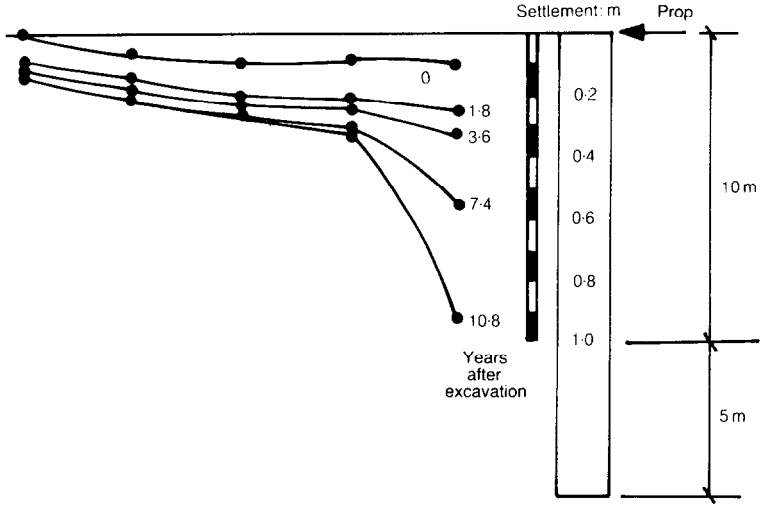

Fig. 28. Soil settlement profiles, test DWC 11

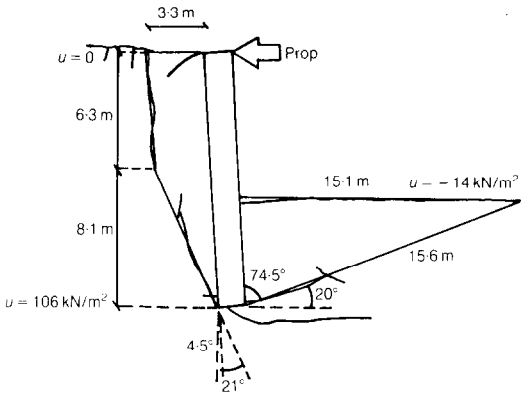

Fig. 29. Idealized rupture surfaces, test DWC 11

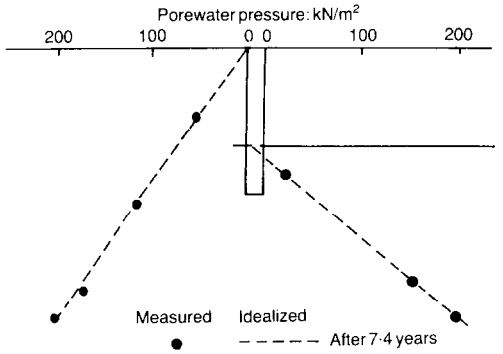

Fig. 30. Measured and idealized long-term porewater pressures, test DWC 11

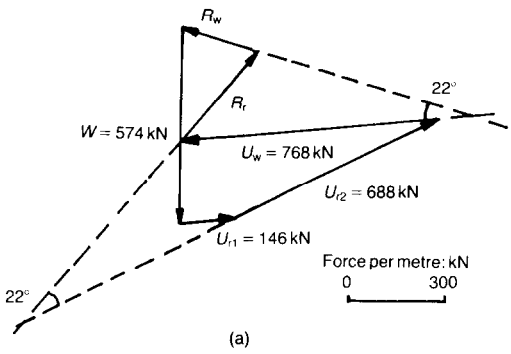

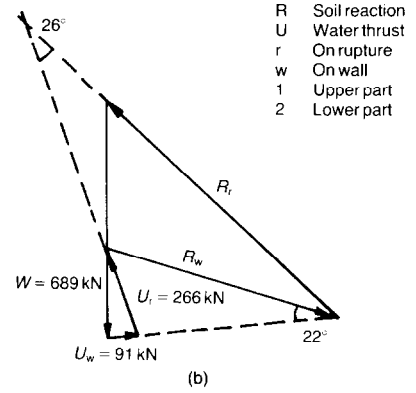

Fig. 31. Polygons of force, test DWC 11: (a) active side; (b) passive side

rupture plane shown in front of the wall in Fig. 29 developed along only a small part of its length, near the toe of the wall. In Fig. 29, it has been extended to meet the excavated soil surface solely for this analysis. The retained height of clay had reduced from 10 m to 8·4 m; this is taken into account in the back analysis.

On the retained side of the wall the wedge of soil defined by the idealized rupture planes is statically indeterminate, even if the directions of the three soil reactions are assumed. However, the direction of the resultant soil reaction on the left-hand side of the wedge is bounded by the two directions associated with the individual rupture planes. Since soil stresses increase both with depth and with rotation of a plane away from the vertical, the direction of the resultant soil reaction will be closer to the direction associated with the lower plane in Fig. 29 than to that associated with the upper plane.

A force polygon for the wedge of soil on the retained side of the wall is shown in Fig. 31. It has been assumed that the resultant soil reaction on the left-hand side is at 22° to the lower rupture plane and that the soil reaction on the right-hand side is at 22° to the wall. A corresponding force polygon for the wedge of soil on the excavated side of the wall is also shown in Fig. 31. The angle of wall friction has been taken as 22°, and a mobilized angle of soil friction of 26° has been invoked along the 'rupture plane'. The latter value is reasonable, since the long rupture plane had not developed along most of its length, so an assumption of complete softening to the critical state would be unjustified. Moreover, it is necessary to assume 26° to satisfy the condition of rotational equilibrium about the prop, taking earth pressures and porewater pressures to vary linearly with depth. Horizontal force equilibrium then dictates a prop load of 220 kN/m. The corresponding bending moments compare favourably with measured values, as shown in Fig. 32. Problems occurred with one of the two prop load cells in this test, so the close correspondence between measured and calculated prop loads should perhaps be treated as fortuitous. Nevertheless, the back analysis of the observed collapse mechanism was broadly satisfactory.

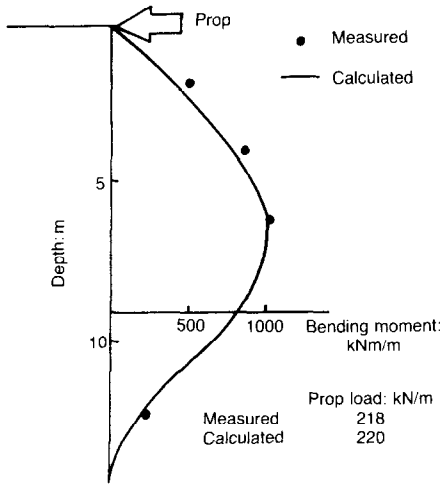

Fig. 32. Structural resultants after 7·4 years (at prototype scale), test DWC 11

The prediction of the rupture of Fig. 27 would not be a simple matter for a designer, however. In particular, the steep active rupture surface could only be generated from an analysis which took account of the effect of the stress distribution against the wall, the restraint to lateral movement of the soil surface as a result of the prop and the angle of dilation mobilized by the soil as it sheared and softened. Any such analysis would be subject to many uncertainties including the degree of soil strain mobilized during construction of a diaphragm wall in the field, the magnitudes of prop and wall flexibility and the long-term effects of the creep of concrete and swelling of soil.

In these circumstances it is more likely that the designer would continue to use earth pressure coefficients which did not take account of the special kinematic restrictions of the propped wall and which therefore erred on the safe side. The equivalent earth pressure coefficients deduced from the thrusts arising from the back analysis of the collapse mechanism, and used in Fig. 32, were 0·23 on the retained side and 4·48 in front of the wall. These coefficients would only be derived from Caquot & Kerisel's (1948) analysis if parameters of the order of $\phi' = 35°$ and $\delta = \phi'_{crit} = 22°$ were employed on the active side and $\phi' = 26°$ and $\delta = 22°$ on the passive side. Such large strengths would not generally be invoked. The overall use of a peak soil strength $\phi' = 28°$ with $\delta = 22°$, for example, would give pressure coefficients of 0·30 on the retained side and 4·45 on the excavated side, which would lead the designer towards anticipating collapse of walls 15% deeper with bending moments 15% greater than those observed in the centrifuge models. Walls must, in any event, be of greater than critical depth to avoid serviceability problems. The economic importance of avoiding conservative collapse calculations may not be large, therefore, if the ruling criterion relates to deformation. Wall displacements and soil deformations will be the subject of a further paper.

CONCLUSIONS

The back analysis of the centrifuge tests has shown that the collapse behaviour of diaphragm walls can be described and explained by the appropriate application of conventional theory. In particular, the following points may be made.

All the unpropped walls were tested with a full height groundwater level and would have been judged unserviceable, if not collapsed, within a short time of excavation. Owing to the large depths of penetration needed for stability, unpropped walls are unlikely to represent an economical method of retaining large (i.e. of the order of 10 m) heights of clay with a full-height groundwater level on the retained side.

It has been demonstrated, both practically and theoretically, that a flooded tension crack provides the severest short-term test of the stability of an unpropped wall in stiff clay. Water might be supplied to the soil–wall interface via the soil surface, a leaking pipe or a sand parting. Under these circumstances, the rate of wall movement will depend on the flow rate of water into the tension crack. The designer of the wall should always be aware of this possibility: stability under these conditions might be viewed as a minimum requirement for any wall, including a temporary construction.

If the soil remains in contact with the wall, short-term equilibrium is maintained by the development of large porewater suctions in the soil immediately adjacent to the wall. The rate at which the wall can move is then governed by the rate at which the soil can shear, change volume or slide along a rupture surface. A fast drainage path into the soil—such as a sand parting—could increase the rate of wall movement considerably.

For the centrifuge models, effective stress calculations based on admissible stress fields switching from active to passive around a pivot point gave a reliable indication of whether or not an unpropped wall would be stable, provided that appropriate porewater pressures and angles of shearing resistance were used in the analysis. There is some evidence that first rupture can be avoided using the peak plane strain angle of shearing resistance of the soil but with zero wall friction. There is more evidence to support the use of the critical state angle for the soil, together with full wall friction, to analyse the ultimate condition of gross displacements.

'Collapse' in the centrifuge models was not a unique or easily identifiable event. Once an initial

state of limiting equilibrium had been reached, the rate of ensuing displacements was dependent on the rate of supply of groundwater to maintain pore pressures. Large changes in geometry then ensued, with local slippages on rupture surfaces. These led to reductions in the height of soil to be retained and increases in the effective depth of penetration, which tended to stabilize the structure.

The designer of a full-scale wall must therefore decide on the totality of conditions which he will assume to represent collapse. In assimilating the results of centrifuge model tests he must take account of the possibility that larger soil slippages at full scale could lead to the further reduction in ϕ' below ϕ'_{crit} and towards a residual value. He may feel that such a situation could occur only after significant geometry changes which would be in his favour. The designer must also be aware that his selection of the angle of wall friction δ, especially in a passive zone, is crucial to the results which will be obtained. Other significant issues will be the estimate of the peak angle of shearing in plane strain and the possibility of progressive failure.

The following scenarios are justifiable tests of stability on the undeformed geometry of an unpropped wall with groundwater at its highest credible level

(*a*) either ϕ'_{max} taken from peak (secant) angle of shearing recorded in undrained triaxial compression tests with pore pressure measurement on samples with the smallest OCR likely to be encountered, and $\delta = 0$

(*b*) or ϕ'_{crit} taken from the angle of shearing resistance in a plane strain or triaxial test consolidated to an effective stress exceeding its precompression, or on reconstituted soil with OCR = 1, and $\delta = \phi'_{crit}$

Soil displacement will be unacceptable if either of these conditions is approached. The assurance of serviceability is a separate topic.

For model walls propped at the crest the kinematic restraint imposed by the prop results in a conservative simple stress field calculation, even when the peak angle of soil shearing resistance ϕ'_{max} is used together with a wall friction angle $\delta = \phi'_{crit}$. A consistent back analysis was obtained for the failure mechanism which was observed, however. Once again, there was an indication that the strength on rupture surfaces fell to the critical state value. A complete rupture did not develop on the passive side, even after substantial wall rotations. The soil's average angle of shearing on the passive side was, accordingly, only marginally less than the estimated peak value. It is possible that a greater degree of progressive failure might occur in the field. Furthermore, it is uncertain that the correct failure mechanism could be predicted. In these circumstances it is likely that designers will opt for the moderate conservatism of using standard earth pressure coefficients together with critical state angles of shearing both in the soil and on the wall surface.

ACKNOWLEDGEMENTS

The first Author was employed by the University of Cambridge. The work reported herein was carried out under a contract placed on him by the Transport and Road Research Laboratory. The views expressed are not necessarily those of the Department of Transport.

The second Author received support from the Science and Engineering Research Council.

The Authors are indebted to I. F. Symons of the Transport and Road Research Laboratory for his advice during the execution of the contract and for his constructive criticism of an earlier draft of the Paper. The Authors also recognize the invaluable support of their colleagues in the Soil Mechanics Group at Cambridge, and in particular the assistance of C. H. Collison, J. Doherty and D. I. Stewart.

REFERENCES

Al-Tabbaa, A. (1987). *Permeability and stress–strain response of speswhite kaolin.* PhD thesis, Cambridge University, to be published.

Bolton, M. D. (1979). *A guide to soil mechanics*, Ch. 10.5. London: Macmillan.

Bolton, M. D. (1986). The strength and dilatancy of sands. *Géotechnique* **36,** No. 1, 65–78.

Caquot, A. & Kerisel, J. (1948). *Tables for the calculation of passive pressure.* Paris: Gauthier-Villars.

Jaky, J. (1944). *The coefficient of earth pressure at rest.* Magyar Mernok es Epitesz Egylet Kozloyne.

Lord, J. A. (1969). *Stresses and strains in an earth pressure problem.* PhD thesis, Cambridge University.

Padfield, C. J. & Mair, R. J. (1984). *Design of retaining walls embedded in stiff clay.* Report 104, Construction Industry Research and Information Association.

Powrie, W. (1985). Discussion on Performance of propped and cantilevered rigid walls. *Géotechnique* **35,** No. 4, 546–548.

Powrie, W. (1986). *The behaviour of diaphragm walls in clay.* PhD thesis, Cambridge University.

Schofield, A. N. (1980). Cambridge Geotechnical Centrifuge operations. 20th Rankine Lecture. *Géotechnique* **30,** No. 3, 227–267.

Sketchley, C. J. (1973). *Behaviour of kaolin in plane strain.* PhD thesis, Cambridge University.

Symons, I. F. (1983). Assessing the stability of a propped in-situ retaining wall in overconsolidated clay. *Proc. Instn Civ. Engrs,* Part 2 **75,** 617–633.

Wroth, C. P. (1972). General theories of earth pressures and deformations. *Proc. 5th Eur. Conf. Soil Mech. Fdn Engng, Madrid* **II,** 33–52.

Wroth, C. P. (1984). The interpretation of in situ soil tests. 24th Rankine Lecture. *Géotechnique* **34,** No. 4, 449–489.